Supporting Information

Thermally-Stable Resistive Switching with Large ON/OFF Ratio Achieved in Poly(Triphenylamine)

Wenbin Zhang,[abd†] Cheng Wang,[c†] Gang Liu,[ad*] Xiaojian Zhu,[ad] Xinxin Chen,[ad] Liang Pan,[ad] Hongwei Tan,[ad] Wuhong Xue,[ad] Zhenghui Ji,[ad] Jun Wang,[b] Yu Chen[c*] and Run-Wei Li,[ad*]

[a]Key Laboratory of Magnetic Materials and Devices, Ningbo Institute of Materials Technology and Engineering, Chinese Academy of Sciences, Ningbo 315201, China

E-mail: liug@nimte.ac.cn ; runweili@nimte.ac.cn

[b]Department of Physics, Ningbo University, Ningbo 315211, China

[c]Institute of Applied Chemistry, East China University of Science and Technology, Shanghai 200237, China
E-mail: chentangyu@yahoo.com

[d]Zhejiang Province Key Laboratory of Magnetic Materials and Application Technology, Ningbo Institute of Materials Technology and Engineering, Chinese Academy of Sciences, Ningbo 315201, China

[†]These authors contribute equally to this work

1. Experiments

1.1 General

All chemicals were purchased from Aldrich (Shanghai, China) and used as received, except otherwise noted. Chloroform was distilled over CaH_2 before use. Weight-average (M_w) and number-average (M_n) molecular weights were determined by a waters 2690 gel permeation chromatography (GPC) using polystyrene standards eluted with tetrahydrofuran (THF, 1 mL/min). The ^{1}H nuclear magnetic resonance (^{1}H NMR) spectra were measured at 400 MHz on a Bruker 400 AVANCE III spectrometer with dimethyl sulfoxide-d_6 (DMSO-d_6) as solvent. Elemental analysis was performed on an Elementar Vario EL III analyzer. The Inductively Coupled Plasma Optical Emission Spectrometer (ICP-OES) (model NEX10N300X) was also used to preclude the existence of $FeCl_3$/$FeCl_2$ residuals in the polymer product. Fourier transform infrared (FTIR) spectra were measured on a Thermo Nicolet 6700 FTIR spectrophotometer by dispersing the samples in KBr pellets. Thermogravimetric analysis (TGA) was conducted on a Perkin-Elmer Diamond TG/DTA instrument at a heating rate of 10 °C/min and under a nitrogen flow rate of 40 mL/min. Differential scanning calorimetry (DSC) measurements were carried out on a Mettler Toledo DSC under N_2 atmosphere and at a heating rate of 10 °C/min. UV-visible absorption and fluorescence spectra of PTPA solution were obtained on a Perkin lambda 950 spectrophotometer and a Hitach-F4600 fluorescence spectrometer, respectively. Cyclic voltammetry (CV) measurements were carried out in an electrolyte solution of tetrabutylammonium perchlorate (n-Bu_4NClO_4) in acetonitrile (0.1 M) under an argon atmosphere, with a platinum gauze and Ag/AgCl as the counter and reference

electrodes respectively. A scan rate of 50 mV/s was used during the CV measurements.

1.2 Synthesis of PTPA

0.05 mol triphenylamine (12.27 g) was first dissolved in $CHCl_3$ in a three-necked flask under magnetic stirring. Then three portions of ferric chloride, each with the amount of 0.05 mol $FeCl_3$ (8.11 g), were sequentially added into the reaction solution at an interval of 1 h. The total amount of ferric chloride used was three times of that of triphenylamine.[1] The oxidative coupling of triphenylamine took another two hours to complete under nitrogen atmosphere. After being cooled down to room temperature, the crude product was collected by precipitation in methanol (400 mL) with stirring. To purify the as-received PTPA, the collected powders were dissolved in $CHCl_3$ again and the insoluble molecules were removed by filtration. The filtrate was concentrated and re-precipitated with acetone containing small amount of aqueous ammonia. Finally, the polymer product was dried in vacuum at 50 °C for 24 h. The yield of PTPA was 70%. The synthesis route of PTPA is shown in **Scheme S1**.

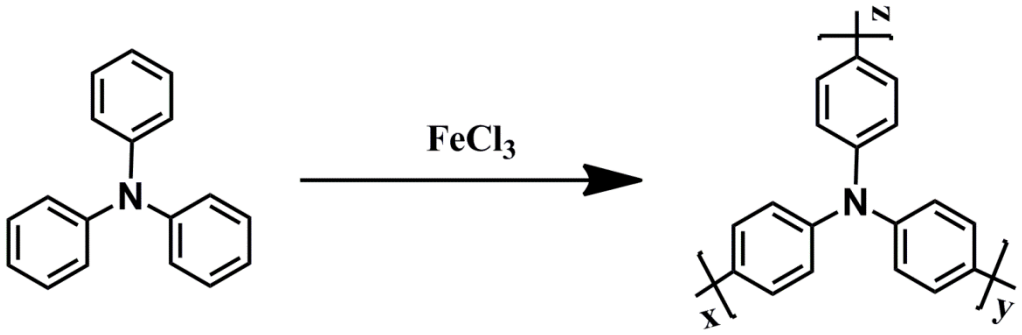

Scheme S1. Synthesis route of PTPA.

1.3 Device fabrication and characterization

The resistive switching behavior of the polymer was examined in the Ta/PTPA/Pt sandwich structured devices. The Pt/Ti/SiO_2/Si substrates (Hefei Ke Jing Materials Technology Co., LTD.) were pre-cleaned with ethanol, acetone and isopropanol in an ultrasonic bath, each for 30 min in that order. The resistance of the Pt/Ti/SiO_2/Si substrate is less than 0.005 Ω·cm. 20 mg PTPA was dissolved in 4 mL chlorobenzene with stirring, and filtrated through a polytetrafluoroethylene (PTFE) membrane micro-filter with a pore size of 0.45 μm to give a homogeneous solution. 50 μL chlorobenzene solution of PTPA was spin-coated onto the substrate at a spinning speed of 600 rpm for 15 s and then at 1000 rpm for 50 s, followed by being vacuum-dried at 80 °C overnight. The thickness of the as-cast polymer film was about 90 nm, as measured by spectroscopic ellipsometer (model M2000DI, Woollam). PTPA films with the thicknesses of 75 nm, 110 nm, 125 nm and 140 nm were also prepared by spin-cast from chlorobenzene solutions with the concentrations of 4.5 mg/mL, 5.5 mg/mL, 6.0 mg/mL and 6.5 mg/mL, respectively. The devices constructed from PTPA films of thicknesses of 75 nm, 90 nm, 110 nm, 125 nm and 140 nm are denoted as PTPA75, PTPA90, PTPA110, PTPA125 and PTPA140, respectively. Ta top electrodes with a diameter of 100 μm and thickness of 60 nm were deposited onto the PTPA film surface at room temperature under reduced pressure (below 10^{-5} Pa), by E-beam evaporation through a metal shadow mask. Tantalum (Ta) and platinum (Pt) are chemically more inert as compared with aluminum (Al) and indium-tin oxide (ITO). Under electric field, Ta or Pt will not react with the polymer switching layer, form interfacial oxide layers or diffuse into the polymer film to form the conductive

filament, either of which may induce resistive switching phenomena. Therefore, to make sure that the observed current-voltage characteristics of the PTPA devices are merely arising from that of the polymer, Ta and Pt-coated Si substrates have been chosen as the top and bottom electrode materials, respectively. The memory performance of the Ta/PTPA/Pt devices was studied using a Keithley 4200 semiconductor characterization system. The precise control of device temperature was achieved with a Model 336 temperature controller, which is a product of the Lakeshore Cryotronics Inc and is installed on the Lakeshore probe station. An input-output feedback system is used to guarantee the precise control of the device temperature. In order to stabilize temperature and avoid any possible influence from the external environment, all the temperature-dependent I-V measurements were carried out in vacuum. The sample device, which was mounted onto the temperature-variant sample stage in the vacuum chamber of the Lakeshore probe station, was first cooled down to and stabilized at 30 K with liquid helium. After being evaluated at 30 K, the device was heated to 70 K and other temperatures precisely, through the counterbalance effect of a built-in heater and the liquid helium refrigeration. The lowest temperature that can be achieved is thus 4K, which is the temperature of liquid helium. The highest temperature than can be achieved in this probe station is 500 K. Generally, the temperature-controlling system will not be operated at full-capacity to avoid over-striking and equipment failure. In our measurement the temperature is controlled in the range of 30 K to 390 K.

The electrical characteristics of the PTPA/Pt structure was also investigated by

conductive-atomic force microscopic (C-AFM) technique, using a Veeco Dimension 3100 V scanning probe microscope. During measurements, the Pt/Ir coated conductive tip was grounded and contacted with the surface of DTPA films and the total measurement areas were fixed at 2×2 μm^2.

1.4 Molecular simulation

Calculations of the optimized geometry and electronic structures, including the dipole moment, highest occupied molecular orbital (HOMO), lowest unoccupied molecular orbital (LUMO) and electrostatic potential (ESP) surface of the basic unit of PTPA, were carried out using the Gaussian 09 program package and density functional theory (DFT) methods at the B3LYP/6-31 G (d) level.[2]

2. Polymer Characterization

The ^{1}H NMR spectrum of PTPA shows signals with the chemical shift of δ 7.65-7.50 (m, 4H), δ 7.45-7.25 (m, 6H) and δ 7.10-6.90 (m, 12H), respectively (**Figure S1**). The FTIR spectrum of PTPA exhibits strong absorption peak at 1485 cm^{-1}, which can be ascribed to the -C=C- stretching vibration of the benzene ring (**Figure S2**). The absorption peak at 1326 cm^{-1} is arising from the stretching vibration of the saturated N-C group. The moderate peaks at 695 cm^{-1}, 750 cm^{-1} and 813 cm^{-1} can be attributed to the characteristics vibration of mono- and 1,4-substitution of the benzene ring.[3,4] The number-average molecular weight (M_n) of PTPA is found to be 2.4×10^3, with a polydispersity index of 1.3 by GPC analysis against a linear polystyrene standard, suggesting that each PTPA macromolecule should carry 10 TPA moieties. The elemental analysis of the polymer confirms that the C:N:H weight ratio of 88.9:6.0:4.9 well agrees with the chemical formula, $C_{180}N_{10}H_{132}$, of the PTPA polymer. Moreover, ICP-OES analysis reveals the residual $FeCl_3/FeCl_2$ existing in the final product is negligible, with only ~ 4.0 ppm of the Fe^{3+}/Fe^{2+} species being present by weight. To ensure the construction of high quality films for better device performance, chlorobenzene with moderate vapor pressure and volatility was used as the solvent,[5] which promises the release of the polymer chain confinement in the solution and the dissipation of the morphological irregularities during spin-coating process.

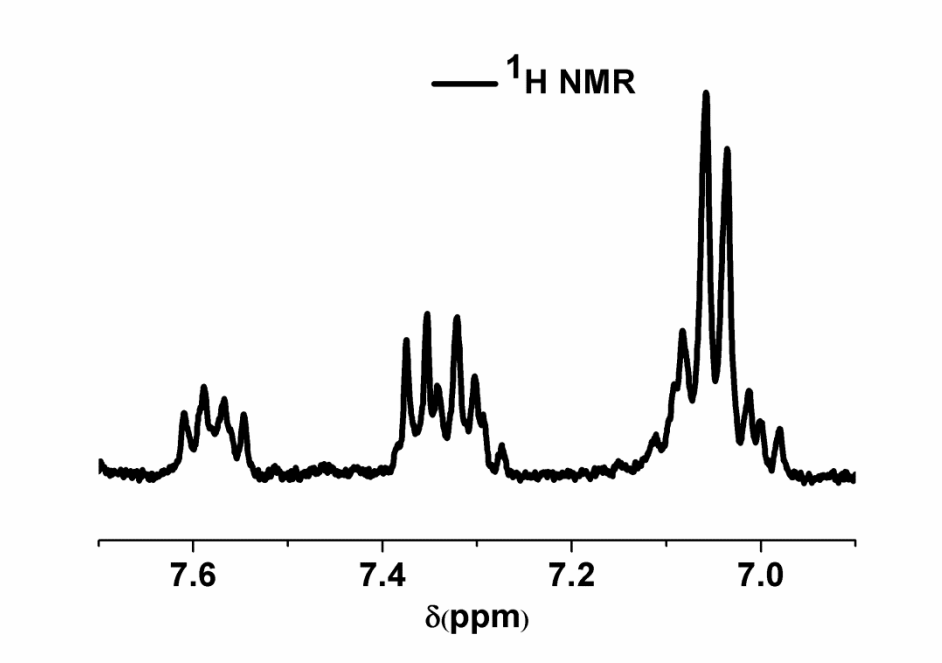

Figure S1. ^{1}H NMR spectrum of PTPA.

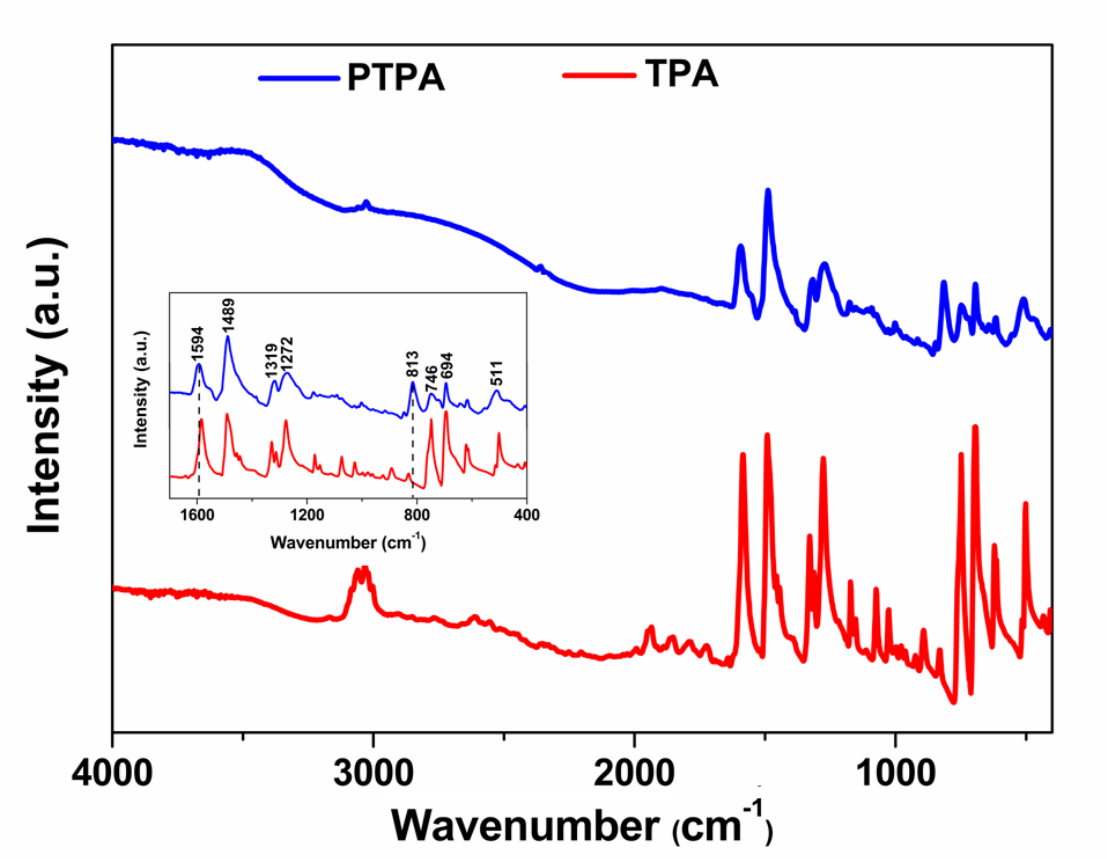

Figure S2. Fourier transformed infrared spectrum of TPA monomer and PTPA polymer.

The FT-IR spectrum of the PTPA polymer shows additional absorption peaks at 813 cm^{-1} and 1594 cm^{-1}, which can be attributed to the C-H out of plane vibration from the 1,4-substited benzene rings and C-C vibration of the quinoid structure, respectively.[3,4] Such absorption peaks are not observed in the FT-IR spectrum of the TPA monomer, therefore proving the successful synthesis of the PTPA polymer.

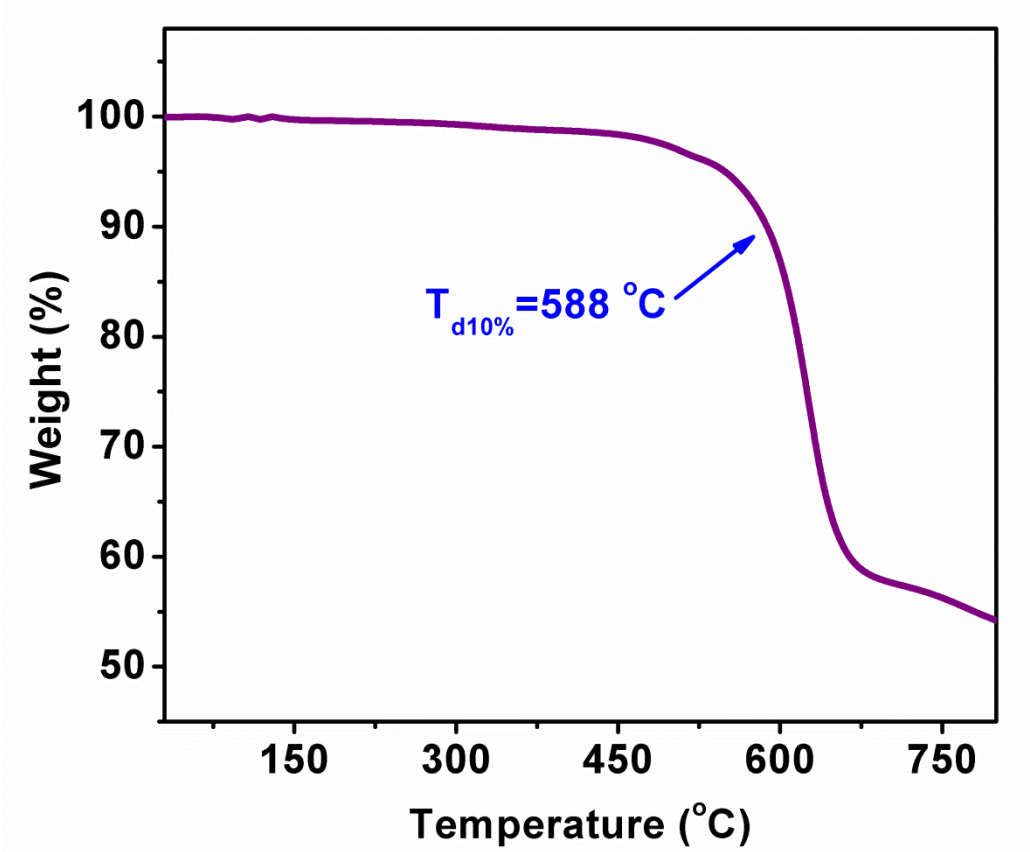

Figure S3. Thermogravimetric curve of PTPA.

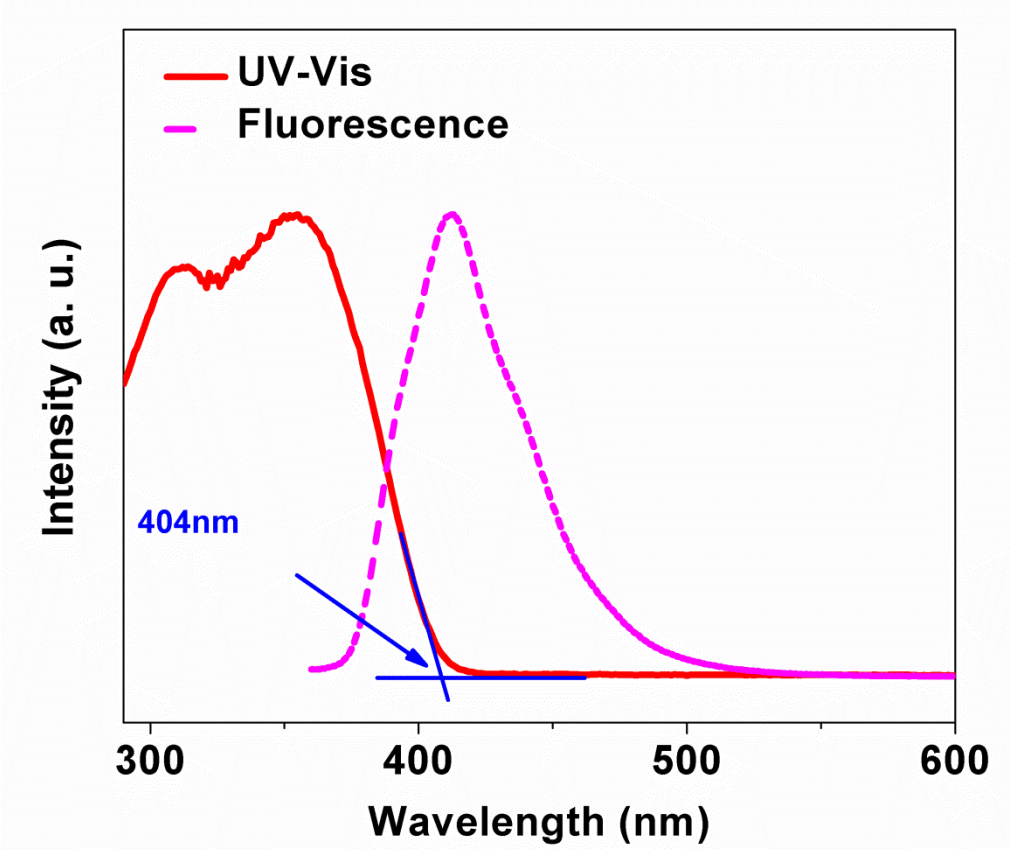

Figure S4. UV-Visible absorption and fluorescence (λ_{ex}=355 nm) spectra of PTPA.

UV-Visible absorption spectrum of PTPA exhibits two absorption peaks at 310 and 353 nm, which are attributed to the π-π* transition of the conjugated backbone, and the coupling between n-π* and π-π* transitions of the arylamine moieties, respectively. The optical band gap of the polymer is estimated from the optical absorption edge of the spectrum with the following equation:

$$E_{op}=hc/\lambda \quad (1)$$

where h is the Planck constant (6.63×10^{-34} m^2kg/s), c is the speed of light (3×10^8 m/s) and λ is optical absorption edge (404 nm). Upon being excited at 355 nm with a continuous laser in the linear optical regime, the polymer gains a strong violet light emission peak at 412 nm, which is arising from the excitonic emission of the non-

interacting arylamine moieties.[6] In accordance with the π-π* absorption of the conjugated backbone, PTPA also shows a respective moderate emission shoulder at 380 nm. Another vibronic emission pattern is also observed at the longer wavelength of 440 nm, which corresponds to the formation of triphenylamine dimers.[7,8] Such dimers can further extend the π-π conjugation of the TPA chromophores and favor the charge carrier transport in solid-state devices.

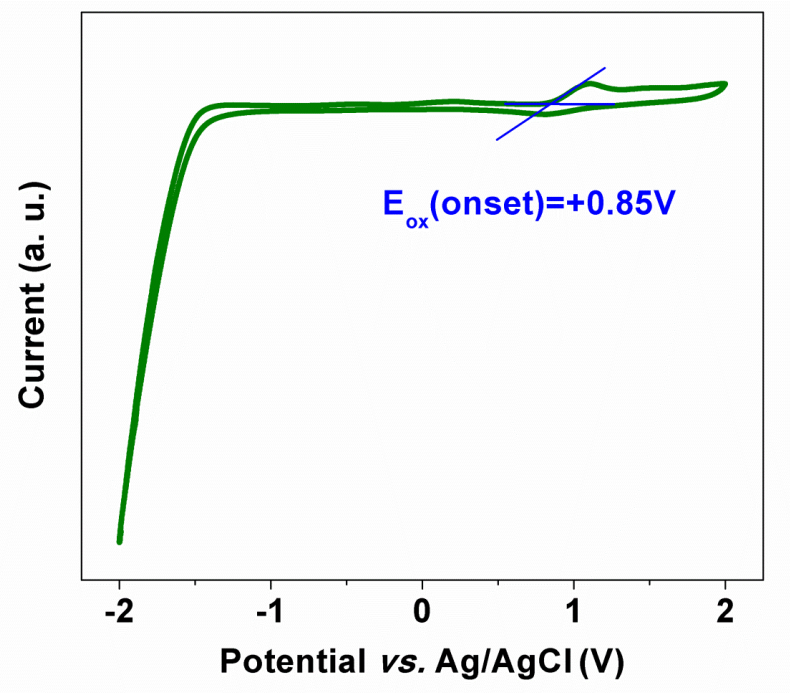

Figure S5. Cyclic voltammogram of PTPA.

The oxidation of PTPA was found with an onset potential of +0.85 V versus Ag/Ag^+, giving rise to a highest occupied molecular orbital (HOMO) energy level of -5.27 eV and a lowest unoccupied molecular orbital (LUMO) energy of -2.20 eV, respectively, according to the following equations:

$$E_{HOMO}=-(E_{ox}(onset)+4.8-E_{FOC}) \quad (2)$$

$$E_{LUMO}=E_{HOMO}+E_g \quad (3)$$

where E_{HOMO} and E_{LUMO} correspond to the energy levels of the HOMO and LUMO, $E_{ox}(onset)$ is the onset oxidation potential of PTPA (+0.85 V), 4.8 is the reference energy of ferrocene (FOC, 4.8 eV under the vacuum level), and E_{FOC} is the potential of FOC/FOC^+ versus Ag/Ag^+ (0.38 eV, measured by cyclic voltammetry). The optical band gap (E_{op}) of the polymer is adopted as the energy band gap E_g to estimate the LUMO energy level.

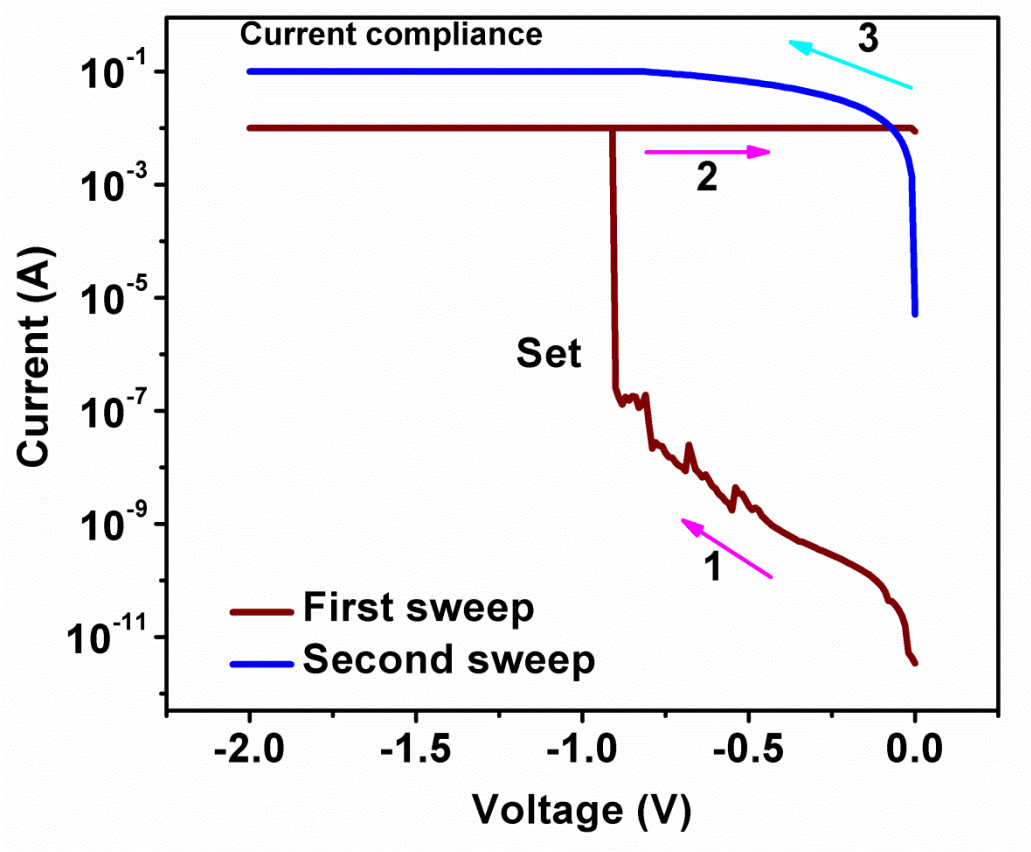

Figure S6. Current-voltage characteristics of the Ta/PTPA90/Pt memory devices in the negative scan with a current compliance of 10^{-1} A.

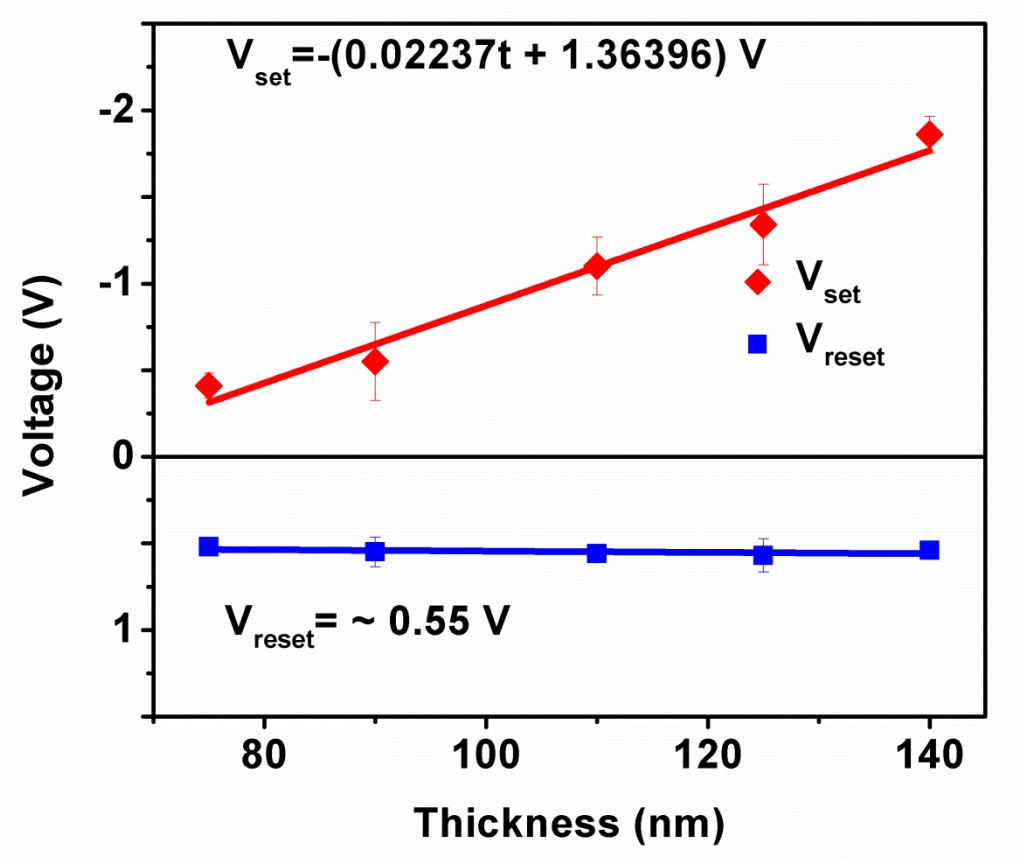

Figure S7. Set/reset voltage-film thickness relationship of the Ta/PTPA/Pt memory devices.

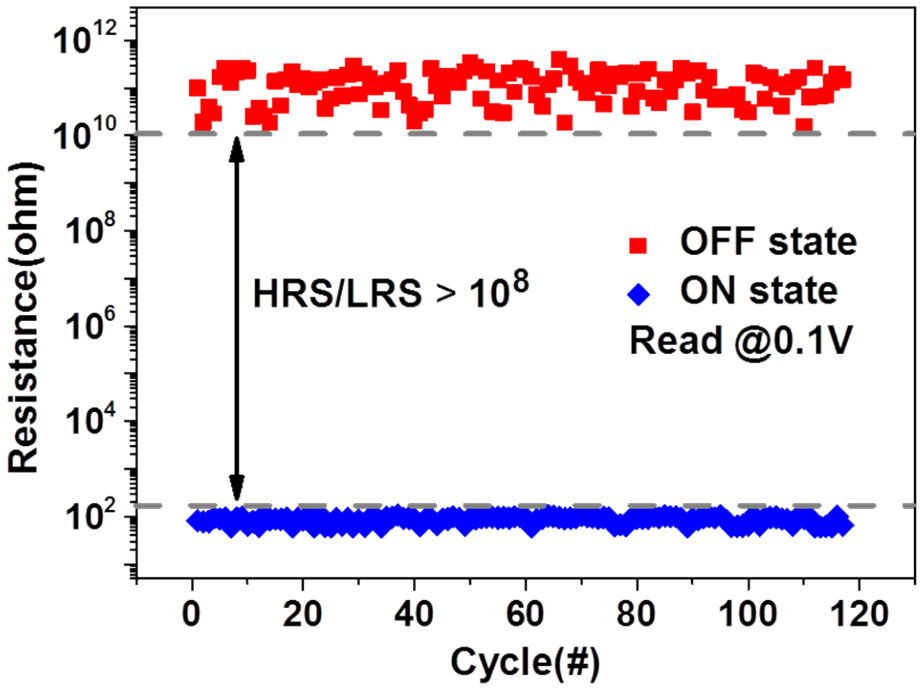

Figure S8. The endurance performance of the Ta/PTPA90/Pt memory device.

The relative high resistance of the OFF state, which is around of ~ 2.5×10^{10} Ω, indicates that the electrode metal atoms do not penetrate into the polymer film during the E-beam deposition procedure. Thus, with the chemically inert nature of the Ta and Pt electrodes, metallic conductive filaments will not be the origin of resistive switching in the present PTPA devices.

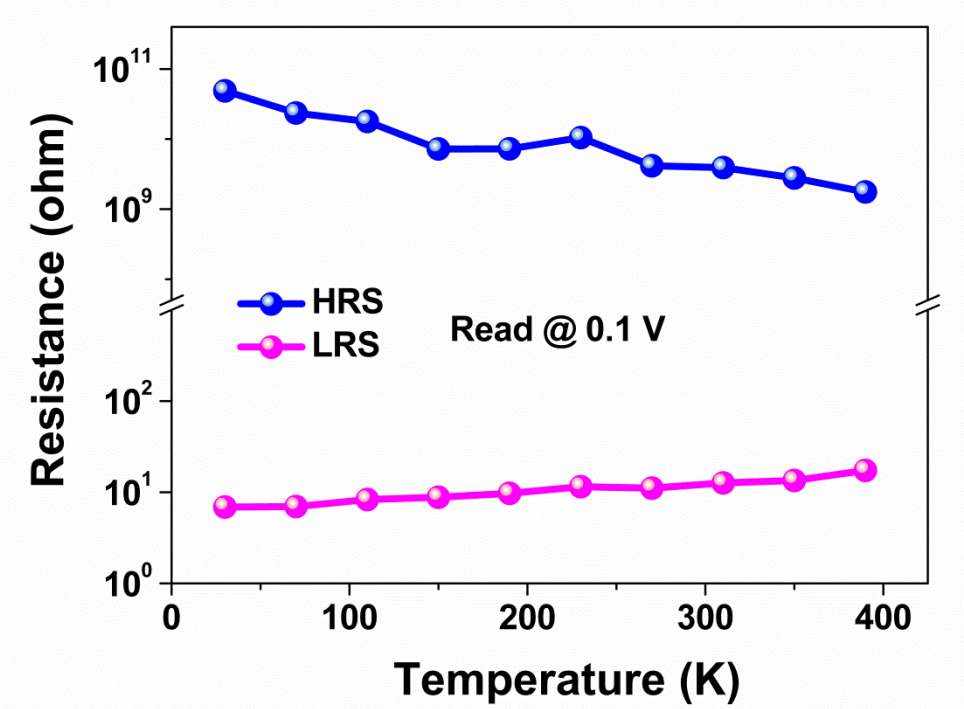

Figure S9. ON and OFF state resistances of the PTPA90 device monitored in the temperature range of 30 K to 390 K.

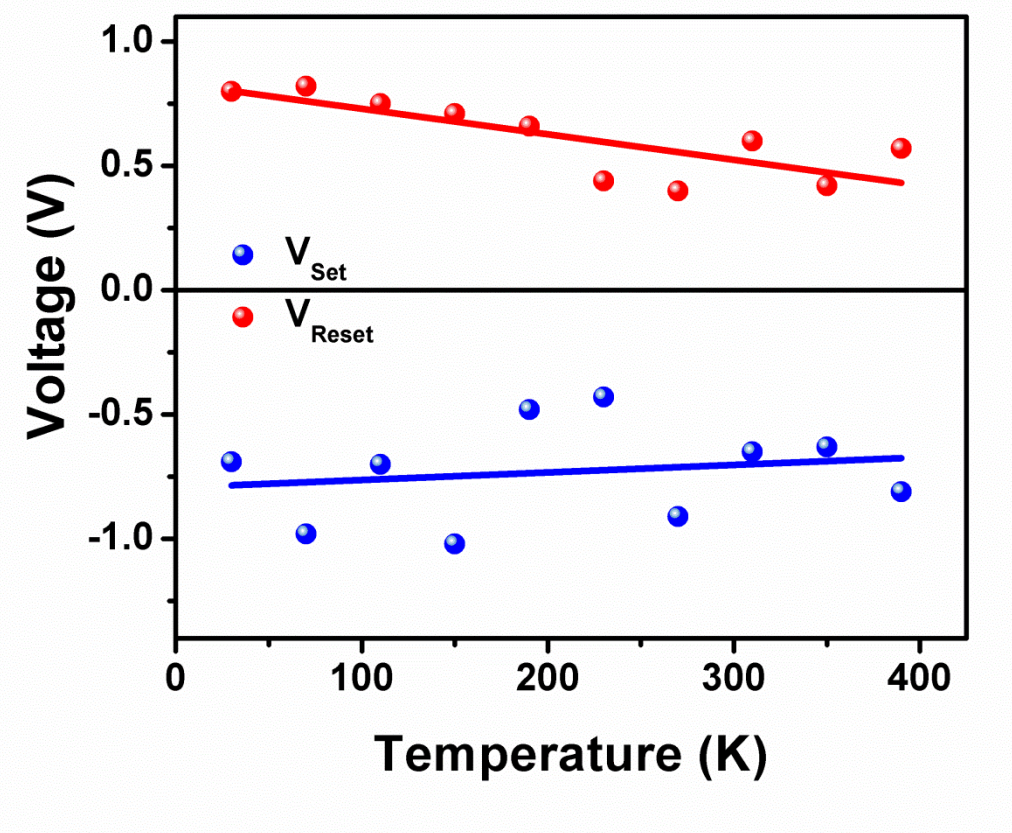

Figure S10. Evolution of the set and reset voltages of the PTPA90 devices in the working temperature range of 30 K to 390 K.

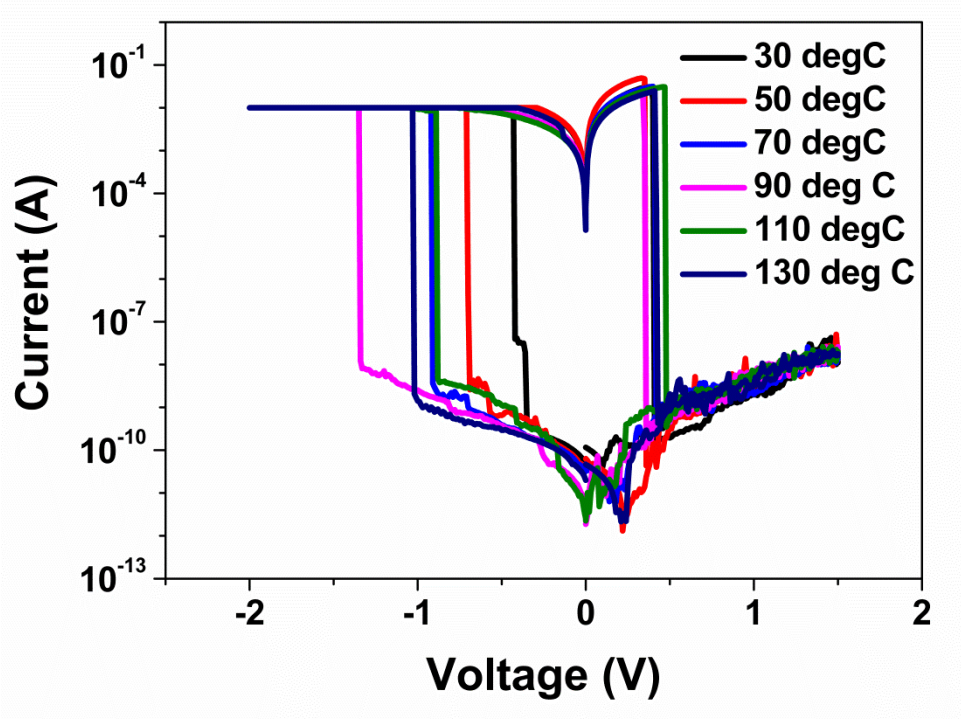

Figure S11. Temperature-dependent current-voltage characteristics of the Ta/PTPA90/Pt device as measured in air.

To further evaluate the thermal stability of the PTPA device, annealing of the Ta/PTPA/Pt structure has been conducted at the temperatures of 30 °C (303 K), 50 °C (323 K), 70 °C (343 K), 90 °C (363 K), 110 °C (383 K) and 130 °C (403 K), respectively, each for 2 h in air. The device resistive switching behavior has been characterized after each annealing operation, and it is found that the device well maintains its memory characteristics. Despite for the minor fluctuation of the set voltages, which may be arising from the interaction between the polymer switching layer and the environmental oxygen/moisture at elevated temperatures, the device resistances in both the ON and OFF states remain almost unchanged. Therefore, the present device does exhibit promising thermal stability, which can be ascribed to the good heat endurance of the PTPA polymer.

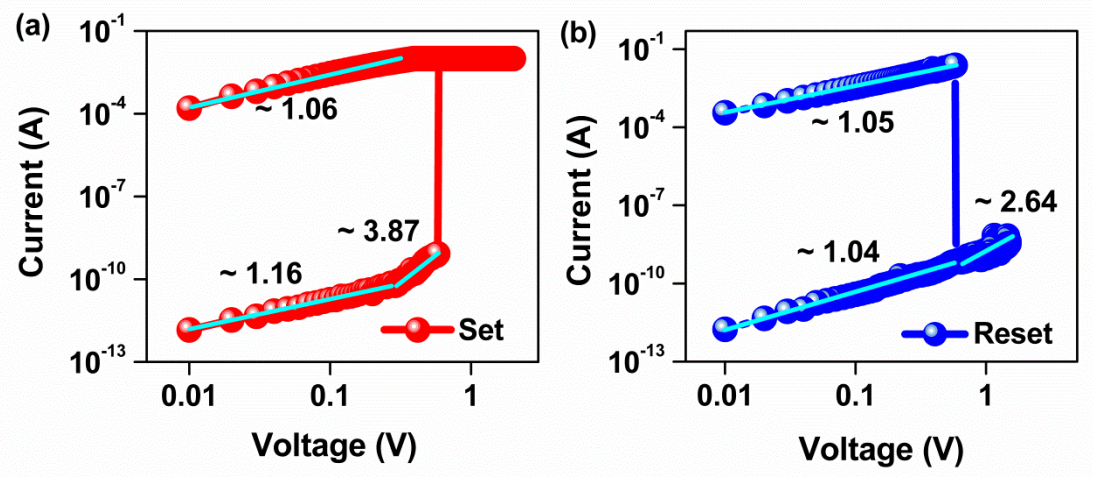

Figure S12. Experimental and fitted I-V characteristics of the PTPA90 devices in the (a) set and (b) reset process.

With the results of molecular simulation supporting the mechanism of charge transfer process (**Figure 3** of the manuscript), the filamentary conducting nature of the polymer film (**Figure 4** of the manuscript), which is revealed by C-AFM analysis, indicates that the occurrence of the charge transfer process is highly localized. This may due to the fact that the electric field distribution inside the polymer film may not be uniform. At the region where the polymer layer/electrode contact shows larger roughness to produce a larger local electric field, the electric field induced charge transfer may occur easier and earlier. Once the CT process occurs in highly localized regions and forms highly conductive pathways, other parts of the polymer film will be short-circuited and no longer be subjected to the external field. Thus the rest parts of the polymer film will not undergo CT and resistive switching processes any more.

To further understand the conduction mechanism, the I-V characteristics of the PTPA devices has been fitted with several theoretical models of Ohmic and space-charge-limited-current (SCLC) conductions as shown in **Figure S12**.[9] The HOMO

and LUMO energy levels of PTPA are -5.27 eV and -2.20 eV, respectively, while the work functions of the Ta and Pt electrodes are -4.25 eV and -5.65 eV, respectively.[10] Therefore, the injection of holes from the Pt electrode into the HOMO of PTPA is energetically favorable and spontaneous, and shows an Ohmic conduction behavior under low electric field (with the slop of ~ 1 in the low field region of the OFF state I-V curve). Further increase of the applied electric field will promote the electron injection from the Al electrode into the polymer film. Consequently, the conduction of the Ta/PTPA/Pt device changes from an Ohmic behavior to a more complicated mode, which may be composed of both the Ohmic and space-charge-limited-current conduction, and shows the slop of ~ 3.87 in the high field region of the OFF state I-V curve. When the applied electric field approaches the threshold, electrons in the HOMO of PTPA will accumulate sufficient energy to transit into the LUMO and get swept to the electrode. Therefore, a highly conductive cationic pathway has been established across the polymer film and switches the device to the ON state. In the ON state, the conduction becomes Ohmic again. However, when a negative sweep with sufficient magnitude has been applied to the device, the cationic conductive pathway will be interrupted with the back transfer of electrons into the HOMO of the polymer, leading to device transition to the OFF state with a SCLC conduction mode showing a slop of ~ 2.64 in the high field region of the OFF state I-V curve again.

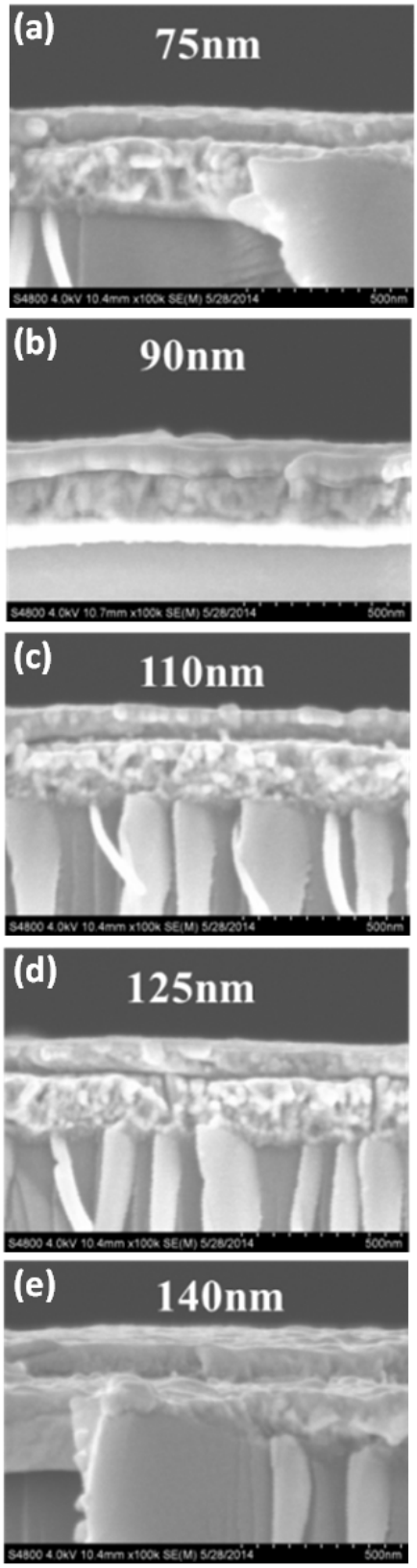

Figure S13. Cross-section scanning electron microscopic images of the PTPA films cast from chlorobenzene solutions with the concentration of (a) 4.5 mg/mL, (b) 5.0 mg/mL, (c) 5.5 mg/mL, (d) 6.0 mg/mL and (e) 6.5 mg/mL, respectively.

3. References

1) J. K. Feng, X. P. Ai, Y. L. Cao, H. X. Yang, *J. Power Sources*, 2006, **161**, 545.

2) M. J. Frish, G. W. Trucks, H. B. Schiegel, G. E. Scuseria, M. A. Robb and J. R. Cheeseman, **Gaussian 09** (Revision A.02), Gaussian Inc., Wallingford CT, 2009.

3) C. M. Zhan, Z. G. Cheng, J. Y. Zheng, W. Zhang, Y. Xi and J. G. Qin, *J. Appl. Polym. Sci.*, 2002, **85**, 2718.

4) C. Kvarnström, A. Petr, P. Damlin, T. Lindfors, A. Ivaska and L. Dunsch, *J. Solid State Electrochem.*, 2002, **6**, 505.

5) P. Müller-Buschbaum, J. S. Gutmann, M. Wolkenhauer, J. Kraus, M. Stamm, D. Smilgies and W. Petry, *Macromolecules*, 2001, **34**, 1369.

6) M. W. Thesen, B. Höfer, M. Debeaux, S. Janietz, A. Wedel, A. Köhler, H.-H. Hohannes and H. Krueger, *J. Polym. Sci. Part A Polym. Chem.*, 2010, **48**, 3417.

7) S. L. Lim, Q. D. Ling, E. Y. H. Teo, C. X. Zhu, D. S. H. Chan, E. T. Kang and K. G. Neoh, *Chem. Mater.*, 2007, **19**, 5148.

8) G. Liu, D.J. Liaw, W. Y. Lee, Q. D. Ling, C. X. Zhu, D. S. H. Chan, E. T. Kang, K. G. Neoh, *Phil. Trans. R. Soc. A*, 2009, **367**, 4203.

9) S. M. Sze, K. K. Ng, *Physics of Semiconductor Devices*, 3rd Ed, 2007, Wiley.

10) W. M. Haynes, *CRC Handbook of Chemistry and Physics*, 92nd Ed, 2011.